Dispersion, damping, and intensity of spin excitations in the monolayer (Bi,Pb)_{2}(Sr,La)_{2}CuO_{6+δ} cuprate superconductor family

Y. Y. Peng, E. W. Huang, R. Fumagalli, M. Minola, Y. Wang, X. Sun, Y. Ding, K. Kummer, X. J. Zhou, N. B. Brookes, B. Moritz, L. Braicovich, T. P. Devereaux, and G. Ghiringhelli

Phys. Rev. B **98**, 144507 — Published 10 October 2018

DOI: 10.1103/PhysRevB.98.144507

Dispersion, damping, and intensity of spin excitations in the single-layer $(Bi,Pb)_2(Sr,La)_2CuO_{6+\delta}$ cuprate superconductor family

Y. Y. Peng,[1,*] E. W. Huang,[2,3] R. Fumagalli,[1] M. Minola,[4] Y. Wang,[3,5] X. Sun,[6] Y. Ding,[6] K. Kummer,[7] X. J. Zhou,[6] N. B. Brookes,[7] B. Moritz,[3] L. Braicovich,[7] T. P. Devereaux,[3] and G. Ghiringhelli[1,8,†]

[1] *Dipartimento di Fisica, Politecnico di Milano, Piazza Leonardo da Vinci 32, I-20133 Milano, Italy*
[2] *Department of Physics, Stanford University, Stanford, California 94305, USA*
[3] *Stanford Institute for Materials and Energy Sciences, SLAC National Accelerator Laboratory and Stanford University, Menlo Park, CA 94025, USA*
[4] *Max-Planck-Institut für Festkörperforschung, Heisenbergstraβe 1, D-70569 Stuttgart, Germany*
[5] *Department of Physics, Harvard University, Cambridge 02138, USA*
[6] *Beijing National Laboratory for Condensed Matter Physics, Institute of Physics, Chinese Academy of Sciences, Beijing 100190, China*
[7] *ESRF, The European Synchrotron, CS 40220, F-38043 Grenoble Cedex, France*
[8] *CNR-SPIN, Politecnico di Milano, Piazza Leonardo da Vinci 32, I-20133 Milano, Italy*

(Dated: September 24, 2018)

Using Cu-L_3 edge resonant inelastic x-ray scattering (RIXS) we measured the dispersion and damping of spin excitations (magnons and paramagnons) in the high-T_c superconductor $(Bi,Pb)_2(Sr,La)_2CuO_{6+\delta}$ (Bi2201), for a large doping range across the phase diagram ($0.03 \lesssim p \lesssim 0.21$). Selected measurements with full polarization analysis unambiguously demonstrate the spin-flip character of these excitations, even in the overdoped sample. We find that the undamped frequencies increase slightly with doping for all accessible momenta, while the damping grows rapidly, faster in the (0,0)→(0.5,0.5) nodal direction than in the (0,0)→(0.5,0) antinodal direction. We compare the experimental results to numerically exact determinant quantum Monte Carlo (DQMC) calculations that provide the spin dynamical structure factor $S(\mathbf{Q},\omega)$ of the three-band Hubbard model. The theory reproduces well the momentum and doping dependence of the dispersions and spectral weights of magnetic excitations. These results provide compelling evidence that paramagnons, although increasingly damped, persist across the superconducting dome of the cuprate phase diagram; this implies that long range antiferromagnetic correlations are quickly washed away, while short range magnetic interactions are little affected by doping.

I. INTRODUCTION

In layered cuprates, doping charge carriers into the CuO_2 planes rapidly suppresses the long-range antiferromagnetic (AF) order of the insulating parent compounds and leads to high critical temperature superconductivity.[1] The proximity of antiferromagnetism to superconductivity in the phase diagram of cuprates and other unconventional superconductors suggests the importance and necessity of a detailed understanding of antiferromagnetism and, more generally, spin excitations. In the absence of long range order, the most important information concerning spin excitations is encoded in their dispersion, intensity, and broadening. Historically, inelastic neutron scattering (INS) was the exclusive technique for studying spin order and excitations in cuprates with momentum and energy resolution. More recently, resonant inelastic x-ray scattering (RIXS), performed at the Cu L_3 resonance,[2–4] has become a promising alternative that complements and extends neutron scattering results due to more favorable cross sections and beam flux that allow for measurements on small crystals, films, and heterostructures.

The largest intensities seen in INS studies correspond to the elastic scattering peak at the AF-ordering wavevector $\mathbf{Q}_{AF}$=(0.5,0.5) in undoped materials and the magnetic resonance of the doped superconducting compounds,[5–8] which rapidly loses intensity in the overdoped regime.[9–11] Generally, INS has demonstrated that around $\mathbf{Q}_{AF}$, both elastic and inelastic scattering due to spin fluctuations are suppressed by doping. Conversely, RIXS measurements have found that spin excitations persist, upon doping, in a large momentum region around the Brillouin zone center Γ=(0,0), even for heavily overdoped, non-superconducting, metallic systems.[12–17] How can we use these results to gain insight on the possible role of spin fluctuations in the formation of Cooper pairs needed for superconductivity? The different trends observed in INS and RIXS can be reconciled by noting that the two techniques primarily access different regions of reciprocal space. As shown by numerical calculations[18,19] of the spin dynamical structure factor $S(\mathbf{Q},\omega)$, the short-range, high-energy spin excitations measured by RIXS close to the magnetic Brillouin zone boundaries are less relevant for pairing than the low-energy ones probed by INS around $\mathbf{Q}_{AF}$. Altogether these findings are consistent with arguments in favor of spin-fluctuations contributing to pairing in cuprate superconductors.[20,21]

Nevertheless, a complete picture has yet to emerge, as most results have focused primarily on the (1,0) antinodal direction, parallel to the Cu-O bonds. In contrast to that behavior, recent experiments have found that the spectra along the (1,1) nodal direction lack easily identifiable collective excitations.[22,23] Interpreted

as charge channel, particle-hole excitations, with support from random-phase approximation (RPA) calculations, these findings challenge the existence of paramagnons (damped collective spin excitations) in doped cuprates.[22–26] The apparent dichotomy between dispersing spin excitations along (1,0), largely insensitive to doping, and a continuum of charge modes along (1,1), which apparently soften upon doping,[24,25] raises questions concerning the doping evolution of magnons into paramagnons and the correct microscopic description of spin excitations in overdoped compounds. The dichotomy may be even more interesting in light of our recent RIXS study demonstrating a direct correlation across several cuprate families between optimal T_c and the difference in dispersion along the (1,0) and (1,1) directions in AF parent compounds,[27] where the difference also correlates with parameters of microscopic models that involve the oxygen degree of freedom, *e.g.* the charge-transfer energy.[28]

While one can debate whether or not a given microscopic model properly describes the low energy physics in the cuprates, these models do provide useful insight on the impact of correlations and their evolution with doping. In particular, recent results from determinant quantum Monte Carlo (DQMC) simulations of the single-band Hubbard model challenge conventional wisdom about that rate at which the influence from correlations decreases with carrier doping.[29] Based solely on single-particle properties,[30,31] one would conclude that correlations weaken rapidly with doping, revealing Fermi-liquid-like behavior just into the overdoped regime. However, the behavior of multi-particle spin and charge response functions shows that the influence from correlations can persist to relatively high doping levels. When compared with the results from RPA calculations, the influence of correlations persists across the Brillouin zone and throughout the doping range relevant to the cuprates. Additional model calculations compared to RIXS experimental results demonstrate a clear delineation between the low energy spin and charge excitations.[32] Given clear distinctions from model calculations, and another recent proposal for a low-energy spin excitation in overdoped cuprates from RPA calculations, which may be resolvable with an improved energy resolution (∼60 meV),[26] an extensive high-resolution study of the doping and momentum dependence of paramagnons may reconcile these differing perspectives.

In this article we present a systematic RIXS study of magnetic excitations in single-layer $(Bi,Pb)_2(Sr,La)_2CuO_{6+\delta}$ (Bi2201), with 4 doping levels ranging from the AF insulator to the overdoped superconductor. Our data cover a significant portion of reciprocal space with an energy resolution of about 55 meV. Polarization-resolved measurements demonstrate the spin-flip nature, even in the overdoped region, of the main spectral feature commonly assigned to paramagnons. We extract the paramagnon dispersion, damping, and spectral weight as functions of momentum and doping by fitting the spectra with a general function

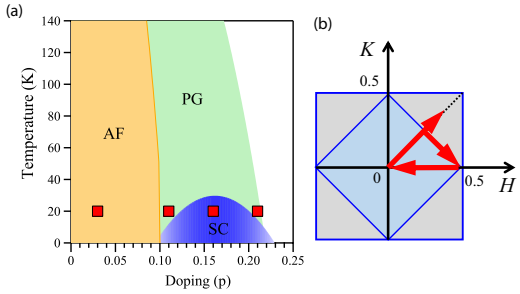

FIG. 1. (a) Schematic temperature-doping phase diagram of $(Bi,Pb)_2(Sr,La)_2CuO_{6+\delta}$. It shows the antiferromagnetic (AF), superconducting (SC) and the pseudogap (PG) regions. Here we study four doping levels as indicated by the solid red squares. (b) 2D reciprocal lattice for the pseudotetragonal structure and the first Brillouin zones (structural in light grey, magnetic in light blue). Coordinates H and K are in r.l.u.. The path followed for the measurements is indicated by the red arrows, starting at (0.25,0.25) and ending around (0.30,0.30) via (0.5,0) and (0,0).

valid for all damping regimes.[22,33] We find that both the undamped frequency and damping factor increase with doping. Moreover, the damping and the spectral weight display a significant momentum dependence. These observations are captured by DQMC calculations of the spin dynamical structure factor $S(\mathbf{Q},\omega)$ for the three-band Hubbard model, which allow us to discuss quantitatively the implications of the experimental results.

II. RIXS EXPERIMENT

A. Experimental details

We have studied four doping levels of Bi2201 as indicated in the phase diagram[34] in Fig. 1(a): antiferromagnetic (AF, $p\simeq 0.03$), underdoped with T_c=15K (UD15K, $p\simeq 0.11$), optimal doping with T_c=33K (OP33K, $p\simeq 0.16$) and overdoped with T_c=11K (OD11K, $p\simeq 0.21$). The sample growth and characterization methods have been reported previously.[35–37] The RIXS measurements were performed with the ERIXS spectrometer at the beam line ID32 of the European Synchrotron Radiation Facility (ESRF) in Grenoble, France.[38] The RIXS spectra were collected at 20K with π incident polarization (parallel to the scattering plane) to maximize the single-magnon signal.[2,39] The scattering angle was fixed at 149.5° and the incident photon energy was tuned to the maximum of the Cu L_3 absorption peak around 931 eV. The total experimental energy resolution was about 55 meV. The samples were cleaved in air a few minutes before installation in the measurement vacuum chamber. The reciprocal lattice units (rlu) used in figures and in text below are defined using the pseudotetragonal unit cell with $a = b = 3.86$ Å. The zero energy-loss position

of each spectrum was determined by measuring, with the same incident photon energy, one nonresonant spectrum of silver paint or carbon tape.

B. RIXS data overview and fitting procedure

Figure 2 displays the energy/momentum intensity maps of RIXS spectra for AF (a), UD15K (b), OP33K (c) and OD11K (d) along the high-symmetry directions indicated in the inset of panel (a). The intensity of RIXS spectra is in unit of photons/s/eV. The magnetic excitations are very sharp for the AF case and become increasingly broader with doping, in agreement with previous results.[12,13,23] The strongly suppressed intensity near $\mathbf{Q}$=(0.5,0) is consistent with the anomalous broadening and damping of spin waves at that momentum in square 2D AF lattice observed previously in, e.g., La_2CuO_4 and in copper deuteroformate tetradeurate by INS [40 and 41] and in $CaCuO_2$ with RIXS, which was ascribed to the decay of spin waves into fractional spin excitations.[42] We note that we do not observe any of the low-energy spin excitation along (0,0)→(0.5,0.5) predicted by the RPA calculations.[26] On the other hand, we have observed a sharp charge-order peak along (0,0)→(0.5,0) direction in the overdoped Bi2201 as reported in Ref. [43]. In the present work we have subtracted out the elastic peak to focus on the study of magnetic excitations.

For a quantitative analysis of these experimental data we have used a general fitting procedure applicable to all cases for the extraction of the energy, intensity and broadening of the spin excitations. The RIXS process leading to a spin excitation can be expressed in terms of the magnetic susceptibility χ, in strict analogy with INS experiments: the spin dynamic structure factor $S(\mathbf{Q},\omega)$ determines the scattering cross section, which is proportional to the imaginary part of the susceptibility $\chi''(\mathbf{Q},\omega)$. The microscopic scattering process is very different for RIXS and INS, so that absolute intensity cannot be directly compared. However their relative intensity can be compared because their dependence on the scattering angles and polarization of the scattering particles are known to evolve slowly with $\mathbf{Q}$ within a given Brillouin zone.[2] Therefore we can fit the RIXS spectra to obtain relevant estimates of the energy, width, and relative intensity of the spin-flip peak and, ultimately, of χ. The fitting function is easily obtained from the expressions of χ and of its imaginary part χ''. For a generic damped harmonic oscillator, of given undamped frequency ω_0 and damping factor γ, it is well known that the complex susceptibility is $\chi(\omega) \propto 1/[(\omega_0^2-\omega^2)+2i\gamma\omega]$. For a given $\mathbf{Q}$ we can thus write

$$\chi''(\mathbf{Q},\omega) \propto \frac{\gamma\omega}{(\omega^2-\omega_0^2)^2+4\gamma^2\omega^2} \qquad (1)$$

When the damping is not too large (i.e. underdamped, $\gamma < \omega_0$) the shape of χ'' can be reproduced by an anti-

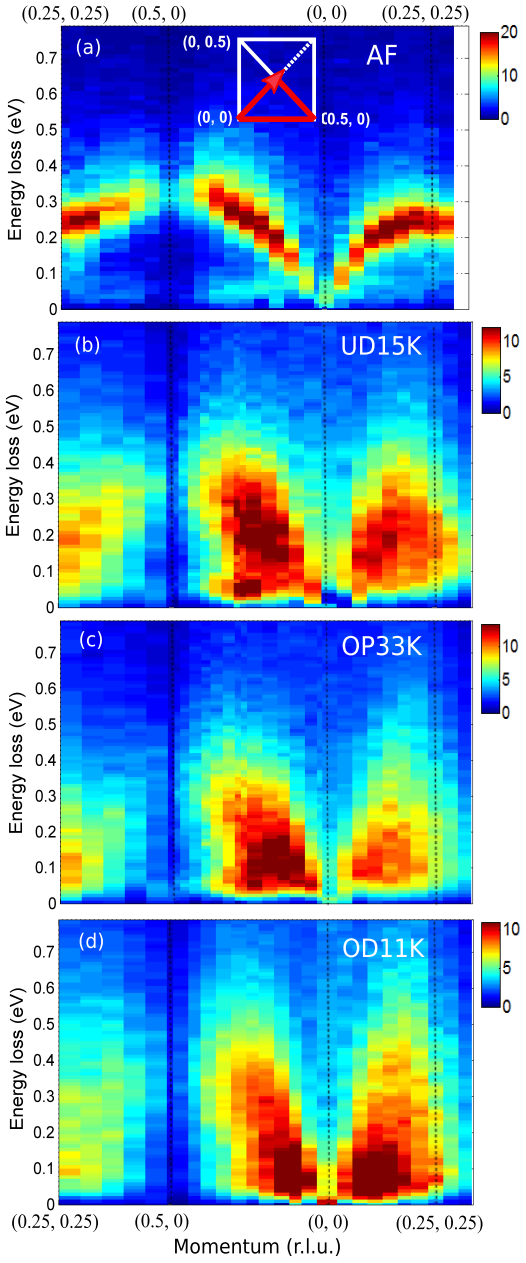

FIG. 2. Energy/momentum intensity maps of RIXS spectra for (a) AF (p≃0.03), (b) UD15K (p≃0.11), (c) OP33K (p≃0.16), and (d) OD11K (p≃0.21) along the high-symmetry momentum trajectory indicated in Fig.1b and in the inset of (a). The intensity is in unit of photons/s/eV. Data were taken with π-polarized incident light at 20 K. Elastic peaks were subtracted for a better visualization of the low energy features.

symmetrized Lorentzian function $L(\omega)$, i.e., the difference of two Lorentzian peaks at position $\pm\omega_p$ and same width γ:

$$L(\omega) = \frac{\gamma}{(\omega-\omega_p)^2+\gamma^2} - \frac{\gamma}{(\omega+\omega_p)^2+\gamma^2} \qquad (2)$$

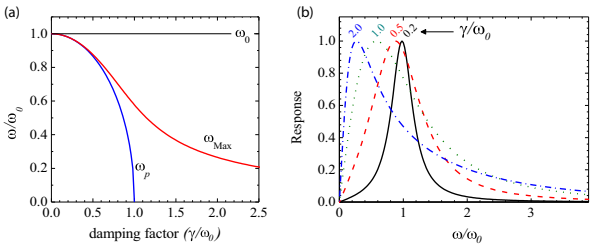

FIG. 3. (a) Illustration of the relative deviation made, for a generic damped oscillator, when using the peak position $\omega_{\rm Max}$ or the central frequency of an antisymmetrized Lorentzian ω_p instead of the actual undamped frequency ω_0, as function of the damping factor γ/ω_0. (b) The effect of damping on the shape of the response of the damped oscillator: the underdamped ($\gamma/\omega_0 = 0.2$, black curve) symmetric peak at $\omega = \omega_0$ moves towards lower frequency for increasing γ. For $\gamma/\omega_0 > 1$ it cannot be fitted anymore by an antisymmetrized Lotentzian with poles at $\omega = \pm\omega_p$ and the spectral shape becomes highly asymmetrical (blue curve, $\gamma/\omega_0 = 2.0$).

Indeed the two functions are identical up to a normalization factor if $\omega_p^2 = \omega_0^2 - \gamma^2$, which is possible only for $\gamma \leq \omega_0$. As pointed out by Lamsal et al.,[33] in some recent RIXS papers[12,13] the antisymmetrized Lorentzian function has been used to fit damped paramagnon curves, leading to an inaccurate estimation of ω_0. The deviation is evident in the case of overdamped paramagnons (i.e. $\gamma > \omega_0$), which cannot be fitted by $L(\omega)$ in a satisfactory way. But even for underdamped paramagnons, that can be fitted well by the antisymmetrized Lorentzian, a non-negligible deviation is made if one assigns to ω_0 the value ω_p obtained from the fitting. It must be also noted that $\omega_{\rm Max}$, the maximum of the function χ'' of Eq. (1), is different from both ω_0 and ω_p when $\gamma \sim \omega_0$ (critically damped), and thus it cannot be used to evaluate "by eye" the undamped frequency either. In Fig. 3 we present the relative deviation of ω_p and $\omega_{\rm Max}$ as function of the damping factor γ/ω_0. Therefore we have consistently fitted all our paramagnon spectra with the function χ'' in Eq. (1), convoluted with the experimental resolution function, obtaining the values of ω_0, γ and relative intensity presented and discussed below.

III. RIXS SPECTRA AND FITTING RESULTS

Figure 4(a,b) show selected examples of fitting for OD11K at the two representative momenta **Q**=(0.4,0) and **Q**=(0.25,0.25). As expected the paramagnon excitation (red line) dominates the mid-infrared range. To validate the assignment of the fitted intensity to spin excitations we exploit the polarimeter of the ERIXS spectrometer.[44] In fact, the spin-flip scattering is accompanied by a 90° rotation of the photon polarization as shown in Fig. 4(e). The polarimeter spectra in Fig. 4(c,d) demonstrate that the crossed polarization channel $\pi\sigma'$

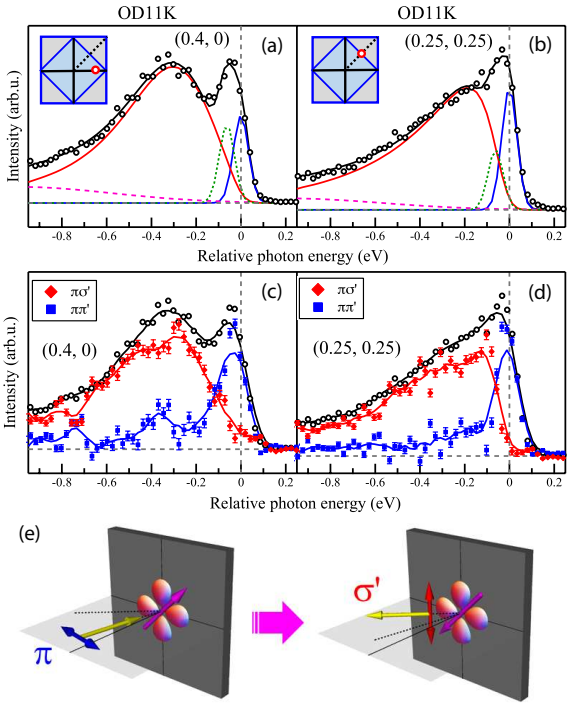

FIG. 4. (a,b) RIXS spectra at (0.4, 0) and (0.25,0.25) respectively, indicated by the red circles in the insets, measured with π-polarized incident light at 20 K for OD11K ($p \simeq 0.21$). The spectra are decomposed into the magnetic excitation (red line), the elastic scattering (blue line), the phonon scattering (green dotted line), and the charge background (dashed magenta line). (c,d) Polarization resolved measurements for OD11K ($p \simeq 0.23$) with incident π-polarized light. Statistical error bars are calculated from the number of photon counts. (e) Schematic illustration of the spin-flip process: the angular momentum conservation requires the 90° rotation of the photon polarization, which has maximum intensity in the $\pi\sigma\prime$ channel at positive momenta (close to normal incidence, grazing emission). The spin conserving processes can be found only in the $\pi\pi\prime$ channel. Here $\sigma\prime$ and $\pi\prime$ refer to the scattered x-ray polarization.

(with σ' refers to the scattered x-ray polarization) dominates the mid-infrared region, even in the absence of a well-defined peak as in **Q**=(0.25,0.25), confirming that the spectra are strongly dominated by spin flip excitations. On the other hand, the quasi-elastic peak is spin-conserving (blue lines for the $\pi\pi'$ scattering), and a non-negligible non-spin-flip intensity is present in the mid-IR region too, due to the charge continuum and to bi-paramagnons.

The raw RIXS spectra for the four dopings are shown in Fig. 5. The magnetic excitations change dramatically: the sharp peaks of the AF sample become broader in UD15K, show loose peak profiles in OP33K, and eventually change to long tails in OD11K. This can be seen most clearly in the bottom spectrum at **Q**=(0.25,0.25): the paramagnon (red shading) changes from a peak in AF to a heavily damped mode in OD11K. We have fit-

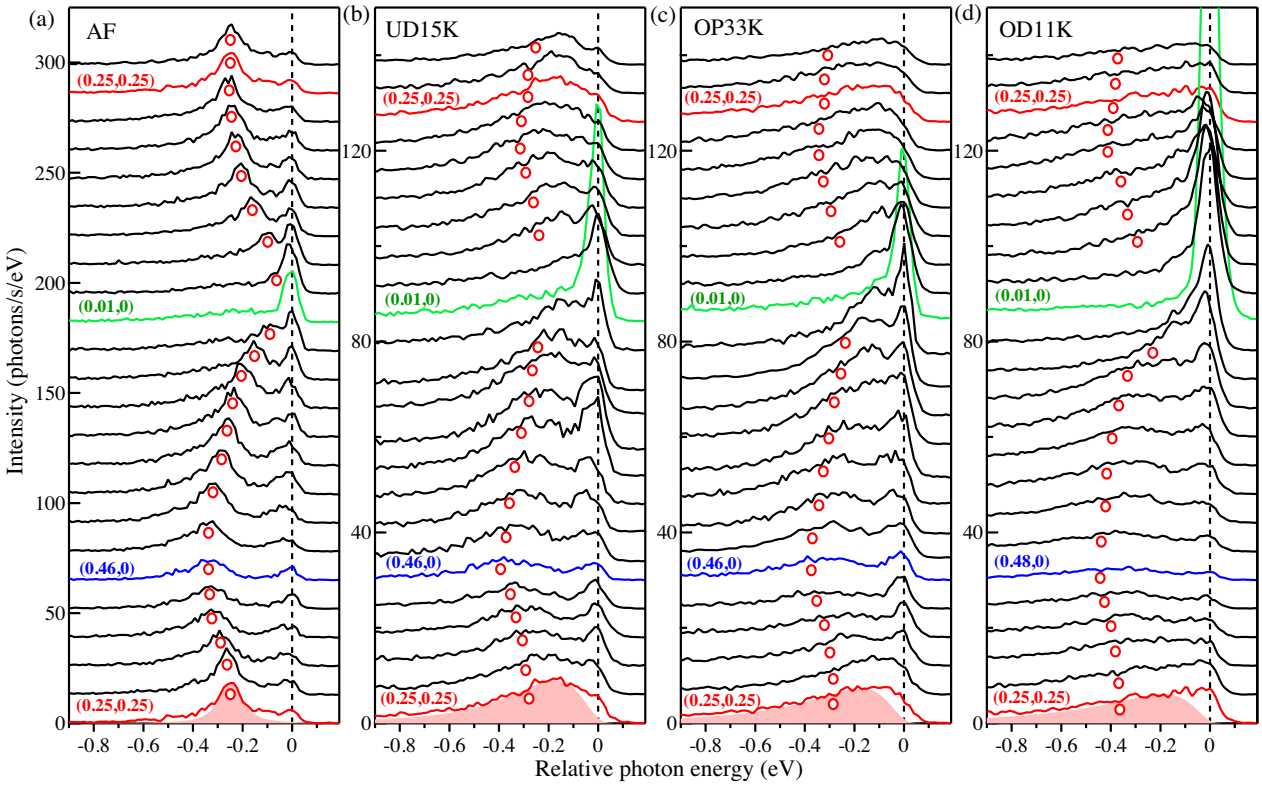

FIG. 5. The raw RIXS spectra for AF (a), UD15K (b), OP33K (c) and OD11K (d) along the high-symmetry directions indicated in Fig. 1b. Each spectrum is shifted vertically for clarity. Circles denote the undamped frequency of magnetic excitations determined from fittings. The red shaded areas in the bottom spectra represent the magnetic excitation.

ted all the spectra with the procedure explained in Set. II. The red circles in the spectra indicate the undamped frequency given by the fitting. The undamped freqency ω_0 and the damping rate γ for all spectra are summarized in Fig. 6. We do not report the fitting results for the spectra very close to (0,0), where the uncertainty is too large due to the elastic peak. The evolution of magnetic excitations with doping and momentum can thus be assessed quantitatively: the dispersion is well defined in AF with small damping rates along the whole trajectory in reciprocal space; in UD15K, the damping increases significantly and becomes comparable with the undamped frequency in the (0,0)→(0.5,0.5) direction; upon further doping, the damping becomes larger than the undamped frequency for OP33K and OD11K along the nodal direction, where paramagnons become overdamped spin-flip modes as demonstrated above with the polarimeter. This is consistent with the recent RIXS study showing how spin excitations in cuprates evolve from collective paramagnons to incoherent spin-flip excitations across optimal doping.[45] Along the AF Brillouin zone direction it is noteworthy that the crossing point between the undamped frequency and the damping moves away from (0.25,0.25) towards (0.5,0) with increasing doping, indicating that the overdamped region expands with doping from the nodal direction, possibly from the AF point (0.5,0.5). The increasing damping factor reflects a shorter mean free distance of magnetic excitations in the Stoner continuum of incoherent electron-hole excitations. The damping increase upon doping seems stronger along the nodal than along the antinodal direction. This fact most likely comes from the increase of the scattering of spin excitations with the electron-hole continuum,[46] as well as from the contribution of incoherent particle-hole excitations to the RIXS spectra,[45] which might be anisotropic in cuprates.

IV. DETERMINANT QUANTUM MONTE CARLO CALCULATION

Here we employ the numerically exact DQMC method[47–50] to study the momentum and doping dependence of $S(\mathbf{Q},\omega)$ for the three-band Hubbard model with a typical set of parameters as given in the caption of Fig. 7. Maximum entropy analytic continuation[51] is used to extract $S(\mathbf{Q},\omega)$ from the imaginary time correlators measured in DQMC. The DQMC calculations show magnetic excitations that persist with doping from p=0.03 to p=0.21 (Fig. 7(a)). Fig. 7(b) shows the spectra at two

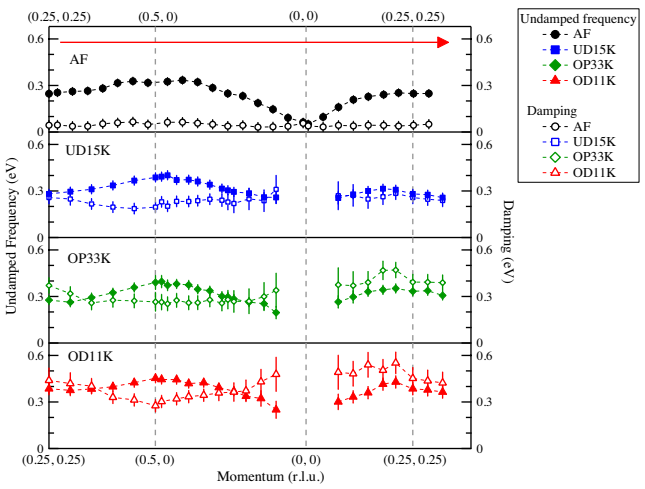

FIG. 6. Doping dependence of undamped frequency ω_0 (solid symbols) and damping γ (hollow symbols) for magnetic excitations along the high-symmetry directions indicated in Fig. 1b. The error bars represent the statistical error from the fitting procedure.

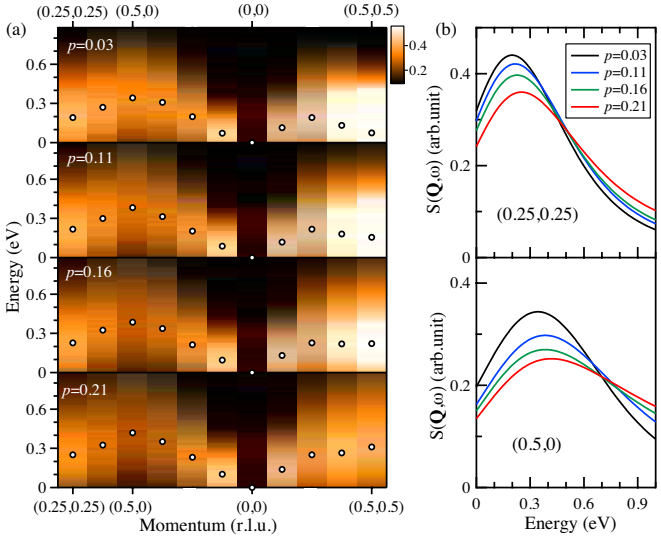

FIG. 7. The spin dynamical structure factor $S(\mathbf{Q},\omega)$ calculated using DQMC for the three-band Hubbard model. (a) False colour plots of the spectra along high-symmetry directions for four dopings $p\simeq$0.03, 0.11, 0.16 and 0.21, respectively. Black circles indicate the peak positions. (b) The $S(\mathbf{Q},\omega)$ at two high symmetry momenta $\mathbf{Q}$=(0.25,0.25) (top panel) and $\mathbf{Q}$=(0.5,0) (bottom panel), showing its evolution with doping. The results were obtained with the three-band Hubbard model (U_d=10.2 eV, U_p=5.9 eV, t_{pd}=1.35 eV, t_{pp}=0.59 eV, Δ=3.9 eV, T= 0.15 eV).

representative momenta, $\mathbf{Q}$=(0.25,0.25) and $\mathbf{Q}$=(0.5,0). The spectral weight of $S(\mathbf{Q},\omega)$ decreases and shifts to higher energy with doping. The broad width of spectra is set predominantly by the high temperature in the simulation. The three-band DQMC calculations correctly reproduce the higher energy of magnetic excitation at $\mathbf{Q}$=(0.5,0) relative to $\mathbf{Q}$=(0.25,0.25), whereas one-band calculations give nearly the same energy at both momenta due to the more Heisenberg-like physics.[18]

V. DISCUSSION

In Figure 8 we compare the experimental and theoretical results. The undamped frequency ω_0 shown in panel (b) is in good agreement with the evolution of the peak position of $S(\mathbf{Q},\omega)$ reported in panel (c): ω_0 increases with doping for all $\mathbf{Q}$ values, in qualitative accord with the DQMC calculations. The agreement is less good only in the neighborhood of (0,0), where the experimental data are more difficult to analyze. On the contrary along the antiferromagnetic zone boundary (AFZB) both experiment and theory find that the dispersion is unaffected by doping, with a rigid shift of the curves to higher energies in the $(0.25,0.25)\rightarrow(0.5,0)$ path, so that the energy difference ΔE=ω_0(0.5,0)-ω_0(0.25,0.25) is almost constant with doping. This is in distinct contrast to the propagation frequency ω_p shown in Fig. 8(a). Along the $(0,0)\rightarrow(0.5,0)$ direction, the propagation frequency decreases slightly with doping, showing a softening behavior as in prior results;[12,13] on the other hand, the propagation frequency along the $(0,0)\rightarrow(0.5,0.5)$ direction decreases significantly in UD15K and goes to zero in OP33K and OD11K, as reported for overdoped $La_{1.77}Sr_{0.23}CuO_4$ [26]. Along the AFZB direction, the propagation energy difference in UD15K increases by $\sim$ 0.1 eV with respect to the AF case. Notably, this is similar to the report of a larger zone-boundary dispersion in underdoped $La_{1.88}Sr_{0.12}CuO_4$ than in the parent compound La_2CuO_4 [22]. It appears evident that the propagation frequency collapses to zero in the nodal direction when reaching the optimal doping, whereas the undamped frequency and, more importantly, the damping grow with doping, thus drastically changing the spectral shape of spin excitations. Therefore the short-range magnetic interaction is little affected by hole doping, but the collective spin excitations (paramagnons) become increasingly damped eventually losing their propagating character.

In Figs. 8(d,e) we compare, for experiment and theory, the intensity variations, with respect to the AF case, upon doping. We normalized the spectral weights to that of the AF cases to avoid possible spurious effects in the measured data, such as self-absorption. The agreement between experimental and numerical trends is remarkably good. The decrease of intensity with doping when approaching $\mathbf{Q}_{\rm AF}$ is due to the disappearance of antiferromagnetic correlation. It is clearly visible in the calculations and known from INS measurements, and is hinted in the RIXS data though they cannot reach $\mathbf{Q}_{\rm AF}$. It has been proposed that the decrease with doping of the spectral weight around $\mathbf{Q}_{\rm AF}$ leads to the reduction of

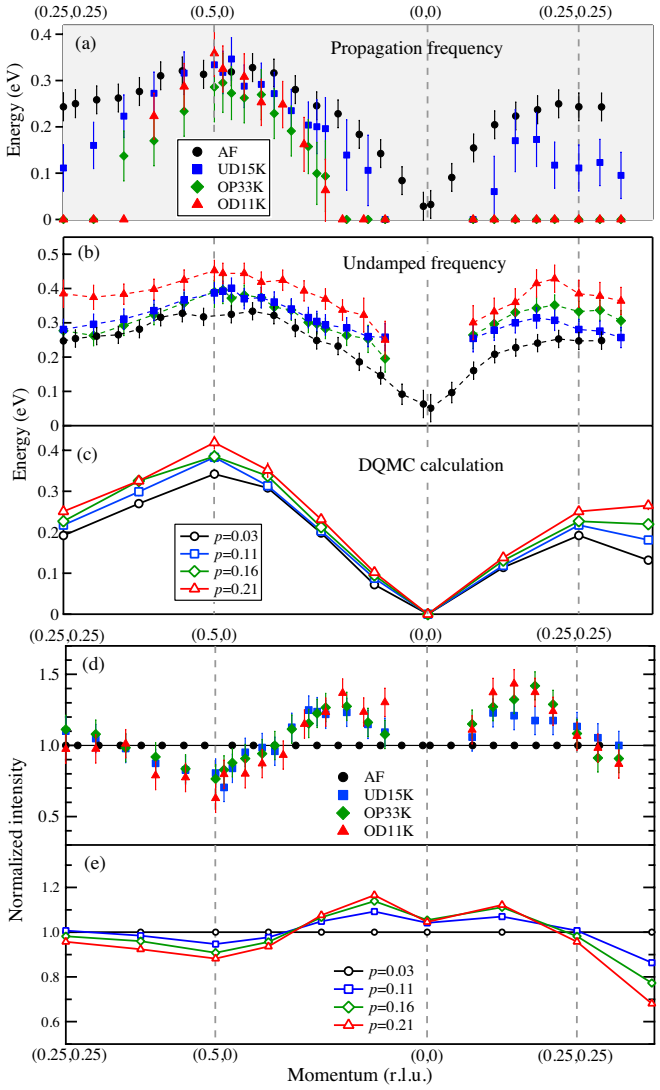

FIG. 8. Comparison of experimental and theoretical results for the spin excitations at 4 doping levels along high symmetry directions. (a) Propagation frequency ω_p and (b) undamped frequency ω_0 from fittings, and (c) peak position of the computed $S(\mathbf{Q},\omega)$. (d) Experimental and (e) calculated intensities normalized, at each momentum, to the magnon intensity for the AF sample / undoped calculated case. The normalization corrects for the momentum dependent self-absorption effects in the experiment and highlights that hole doping increases short-range spin correlation and destroys the long-range one.

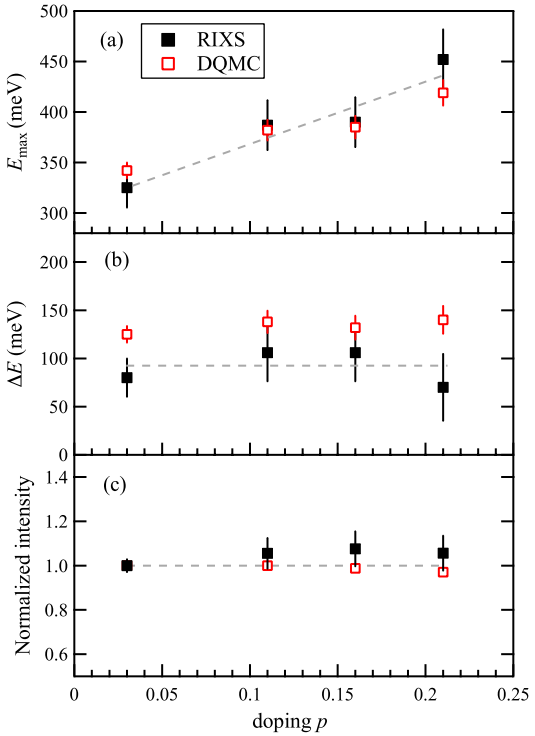

FIG. 9. Doping dependence of (a) the zone boundary undamped frequency $E_{\rm max}$=ω_0(0.5,0), (b) the energy dispersion along the AF zone boundary ΔE=ω_0(0.5,0)-ω_0(0.25,0.25), and (c) the sum of the relative intensities of Fig. 8(d,e). The solid squares are from experiments and hollow squares are from DQMC calculations. Dashed lines are guides for the eye.

the d-wave spin-fluctuation pairing strength.[19] More surprisingly, we find that the intensity decreases at (0.5,0) and increases around (0,0), probably due to a strengthening of the ferromagnetic correlation that would peak at $\mathbf{Q}=0$. This is in accordance with the occurrence of the two-dimensional ferromagnetic fluctuations observed in overdoped Bi2201 [52], suggesting the magnetic ground state changes from antiferromagnetic to ferromagnetic with increasing doping. Remarkably, the resulting crossing points coincide in experiment and theory around $(0.35,0)$ and $(0.25,0.25)$.

Figure 9 gives an overview of the doping dependence of magnetic excitation properties, showing a very good agreement between RIXS experiments and DQMC calculations. The undamped frequency at the boundary $E_{\rm max}$=ω_0(0.5,0) increases with doping, while the energy dispersion along the AFZB, i.e. ΔE, remains substantially unchanged with doping. The hardening of $E_{\rm max}$ with doping is effected by the three-site exchange term, which increases the overall energy cost of spin excitations to break both spin exchange and three-site bonds.[18] Although a discrepancy in the absolute value of ΔE between calculation and experiment is still present and might be reduced by tuning the parameters used in the simulation, the overall constant trend vs. doping is already very similar. This result can be explained by noting that ΔE is determined by the bare parameters related to the charge-transfer energy, which is not significantly modified with doping. Our recent RIXS study on undoped cuprates demonstrated ΔE was positively correlated with the range of in-plane exchange couplings.[27] The marginal changes in ΔE upon doping imply that the exchange-coupling ranges are encoded in the parent

compounds.

On the other hand, the energy- and momentum-integrated intensity of paramagnons in the range accessible to RIXS is found to be constant with doping, even though the spectral weight at $\mathbf{Q}_{\rm AF}$ drops due to the falloff of antiferromagnetism. This indicates that spectral weight away from $\mathbf{Q}_{\rm AF}$ redistributes upon doping while roughly maintaining a constant total weight. While this is generally in line with previous RIXS results on the persistence of spin excitations upon doping,[12,13,23] this observation is not immediately obvious from any sum-rule-type or similar analysis. On the contrary, INS data at $\mathbf{Q}_{\rm AF}$ would rather suggest a general decrease of the spin spectral weight.

VI. CONCLUSIONS

In summary, we have revealed that the short and mid range exchange interaction is relatively little affected by doping. This can be seen by the flatness of ΔE and by the increase of the maximum of the paramagnon energy at (0.5,0), largely due to the contribution from the three-site exchange that overcompensate for the decrease of effective magnetic neighbouring sites. The melting of the long range AF correlation is encoded in the sharp increase of the damping. Spin excitations get increasingly coupled to charge modes and cannot propagate more than few lattice units in plane, although their exceptionally high energy is fully preserved even in the overdoped samples. The three-band DQMC calculation reproduces qualitatively the paramagnon dispersions and intensity dependence with doping and momentum. By studying the three-band Hubbard model, and not making a priori assumptions about the importance of various spin-exchange processes, we have a thorough microscopic description of the electronic degrees of freedom in the CuO_2 layers, with calculations capturing the same electronic effects and processes revealed by the RIXS experiment.

It is interesting to make a connection between the variation of T_c with doping and the overall evolution of the spin fluctuation spectra measured here. In a weak coupling picture in which the spin fluctuation spectrum is treated as the pairing boson in analogy with phonons in conventional superconductors, the redistribution of spectral weight shown in Figure 8 would have a strong effect on the d-wave pairing interaction. Since spin fluctuations carrying momenta $\mathbf{Q}_{\rm AF}$ contribute largest to the pairing interaction, and those with $\mathbf{Q} \sim 0$ give a negative contribution to pairing, one can infer from our results that the overall strength of pairing decreases with doping as spectral weight transfers towards ferromagnetic correlations over anti-ferromagnetic ones. This is irrespective of the effect of damping of paramagnons, which only redistributes spectral weight in energy and is a subdominant effect compared to the momentum-dependent spectral weight transfer. However we caution that this conclusion can only be speculative. For example it is known from many numerical studies that various candidate ground states having different orders - in the form of stripes, charge/spin order, as well as superconductivity all exist at relatively the same energy, and therefore a full understanding of superconductivity would not be captured from simply an examination of the spin fluctuation spectra alone. Indeed recent calculations suggest an intimate coupling between charge density waves (stripes) and superconducting order in the single-band Hubbard model.[53] It would be quite useful to likewise perform an analysis of the charge degrees of freedom to further investigate a connection to superconductivity. This remains a topic for future study.

ACKNOWLEDGMENTS

We acknowledge insightful discussions with Matthieu Le Tacon, Mark Dean, Krzysztof Wohlfeld and José Lorenzana. The experimental data were collected at the beam line ID32 of the European Synchrotron (ESRF) in Grenoble (F) using the ERIXS spectrometer designed jointly by the ESRF and Politecnico di Milano. This work was supported by ERC-P-ReXS project (2016-0790) of the Fondazione CARIPLO and Regione Lombardia, in Italy. M. M. was partially supported by the Alexander von Humboldt Foundation. XJZ thanks financial support from the National Natural Science Foundation of China (11334010 and 11534007), the National Key Research and Development Program of China (2016YFA0300300) and the Strategic Priority Research Program (B) of Chinese Academy of Sciences (XDB07020300). EWH, YW, BM, and TPD were supported by the U.S. Department of Energy (DOE), Office of Basic Energy Sciences, Division of Materials Sciences and Engineering, under Contract No. DE-AC02-76SF00515. Computational work was performed on the Sherlock cluster at Stanford University and on resources of the National Energy Research Scientific Computing Center, supported by the U.S. DOE under Contract No. DE-AC02-05CH11231.

* pyy2018@illinois.edu; Present address: Department of Physics and Seitz Materials Research Laboratory, University of Illinois, Urbana, IL 61801, USA

† giacomo.ghiringhelli@polimi.it

[1] P. A. Lee, N. Nagaosa, and X. G. Wen, Rev. Mod. Phys. **78**, 17 (2006).

[2] L. J. P. Ament, G. Ghiringhelli, M. M. Sala, L. Braicovich, , and J. van den Brink, Phys. Rev. Lett. **103**, 117003

(2009).
[3] M. W. Haverkort, Phys. Rev. Lett. **105**, 167404 (2010).
[4] L. Braicovich, J. van den Brink, V. Bisogni, M. M. Sala, L. J. P. Ament, N. B. Brookes, G. M. D. Luca, M. Salluzzo, T. Schmitt, V. N. Strocov, and G. Ghiringhelli, Phys. Rev. Lett. **104**, 077002 (2010).
[5] H. F. Fong, B. Keimer, D. L. Milius, and I. A. Aksay, Phys. Rev. Lett. **78**, 713 (1997).
[6] H. F. Fong, P. Bourges, Y. Sidis, L. P. Regnault, A. Ivanov, G. D. Gu, N. Koshizuka, and B. Keimer, Nature **398**, 588 (1999).
[7] H. He, P. Bourges, Y. Sidis, C. Ulrich, L. Regnault, S. Pailhes, N. S. Berzigiarova, N. N. Kolesnikov, and B. Keimer, Science **295**, 1045 (2002).
[8] G. Yu, Y. Li, E. M. Motoyama, X. Zhao, N. Barišić, Y. Cho, P. Bourges, K. Hradil, R. A. Mole, , and M. Greven, Phys. Rev. B **81**, 064518 (2010).
[9] S. Wakimoto, H. Zhang, K. Yamada, I. Swainson, H. Kim, and R. J. Birgeneau, Phys. Rev. Lett. **92**, 217004 (2004).
[10] S. Wakimoto, K. Yamada, J. M. Tranquada, C. D. Frost, R. J. Birgeneau, and H. Zhang, Phys. Rev. Lett. **98**, 247003 (2007).
[11] M. Fujita, H. Hiraka, M. Matsuda, M. Matsuura, J. M. Tranquada, S. Wakimoto, G. Y. Xu, and K. Yamada, J. Phys. Soc. Jpn **81**, 011007 (2012).
[12] M. L. Tacon, G. Ghiringhelli, J. Chaloupka, M. M. Sala, V. Hinkov, M. W. Haverkort, M. Minola, M. Bakr, K. J. Zhou, S. Blanco-Canosa, C. Monney, Y. T. Song, G. L. Sun, C. T. Lin, G. M. D. Luca, M. Salluzzo, G. Khaliullin, T. Schmitt, L. Braicovich, and B. Keimer, Nat. Phys. **7**, 725 (2011).
[13] M. P. M. Dean, G. Dellea, R. S. Springell, F. Yakhou-Harris, K. Kummer, N. B. Brookes, X. Liu, Y.-J. Sun, J. Strle, T. Schmitt, L. Braicovich, G. Ghiringhelli, I. Bozovic, and J. P. Hill, Nat. Mater. **12**, 1019 (2013).
[14] M. P. M. Dean, A. J. A. James, R. S. Springell, X. Liu, C. Monney, K. J. Zhou, R. M. Konik, J. S. Wen, Z. J. Xu, G. D. Gu, V. N. Strocov, T. Schmitt, and J. P. Hill, Phys. Rev. Lett. **110**, 147001 (2013).
[15] M. L. Tacon, M. Minola, D. C. Peets, M. M. Sala, S. BlancoCanosa, V. Hinkov, R. Liang, D. A. Bonn, W. N. Hardy, C. T. Lin, T. Schmitt, L. Braicovich, G. Ghiringhelli, and B. Keimer, Phys. Rev. B **88**, 020501 (2013).
[16] Y. Y. Peng, M. Hashimoto, M. M. Sala, A. Amorese, N. B. Brookes, G. Dellea, W.-S. Lee, M. Minola, T. Schmitt, Y. Yoshida, K.-J. Zhou, H. Eisaki, T. P. Devereaux, Z.-X. Shen, L. Braicovich, and G. Ghiringhelli, Phys. Rev. B **92**, 064517 (2015).
[17] M. Minola, G. Dellea, H. Gretarsson, Y. Y. Peng, Y. Lu, J. Porras, T. Loew, F. Yakhou, N. B. Brookes, Y. B. Huang, J. Pelliciari, T. Schmitt, G. Ghiringhelli, B. Keimer, L. Braicovich, and M. L. Tacon, Phys. Rev. Lett. **114**, 217003 (2015).
[18] C. J. Jia, E. A. Nowadnick, K. Wohlfeld, Y. F. Kung, C.-C. Chen, S. Johnston, T. Tohyama, B. Moritz, and T. P. Devereaux, Nat. Commun. **5**, 3314 (2014).
[19] E. W. Huang, D. J. Scalapino, T. A. Maier, B. Moritz, and T. P. Devereaux, Phys. Rev. B **96**, 020503 (2017).
[20] D. J. Scalapino, Rev. Mod. Phys. **84**, 1383 (2012).
[21] T. Dahm, V. Hinkov, S. V. Borisenko, A. A. Kordyuk, V. B. Zabolotnyy, J. Fink, B. Büchner, D. J. Scalapino, W. Hanke, and B. Keimer, Nat. Phys. **5**, 217 (2009).
[22] O. Ivashko, N. E. Shaik, X. Lu, C. G. Fatuzzo, M. Dantz, P. G. Freeman, D. E. McNally, D. Destraz, N. B. Christensen, T. Kurosawa, N. Momono, M. Oda, C. E. Matt, C. Monney, H. M. Rønnow, T. Schmitt, and J. Chang, Phys. Rev. B **95**, 214508 (2017).
[23] D. Meyers, H. Miao, A. C. Walters, V. Bisogni, R. S. Springell, M. d'Astuto, M. Dantz, J. Pelliciari, H. Y. Huang, J. Okamoto, D. J. Huang, J. P. Hill, X. He, I. Božović, T. Schmitt, and M. P. M. Dean, Phys. Rev. B **95**, 075139 (2017).
[24] M. Guarise, B. D. Piazza, H. Berger, E. Giannini, T. Schmitt, H. M. Rønnow, G. A. Sawatzky, J. van den Brink, D. Altenfeld, I. Eremin, and M. Grioni, Nat. Commun. **5**, 5760 (2014).
[25] M. P. M. Dean, A. J. A. James, A. C. Walters, V. Bisogni, I. Jarrige, M. Hücker, E. Giannini, M. Fujita, J. Pelliciari, Y. B. Huang, R. M. Konik, T. Schmitt, and J. P. Hill, Phys. Rev. B **90**, 220506 (2014).
[26] C. Monney, T. Schmitt, C. E. Matt, J. Mesot, V. N. Strocov, O. J. Lipscombe, S. M. Hayden, and J. Chang, Phys. Rev. B **93**, 075103 (2016).
[27] Y. Y. Peng, G. Dellea, M. Minola, M. Conni, A. Amorese, D. D. Castro, G. M. D. Luca, K. Kummer, M. Salluzzo, X. Sun, X. J. Zhou, G. Balestrino, M. L. Tacon, B. Keimer, L. Braicovich, N. B. Brookes, and G. Ghiringhelli, Nat. Phys. **13**, 1201 (2017).
[28] Y. Wang, E. W. Huang, B. Moritz, and T. P. Devereaux, Phys. Rev. Lett. **120**, 246401 (2018).
[29] Y. F. Kung, E. A. Nowadnick, C. J. Jia, S. Johnston, B. Moritz, R. T. Scalettar, and T. P. Devereaux, Phys. Rev. B **92**, 195108 (2015).
[30] M. Kohno, Phys. Rev. Lett. **108**, 076401 (2012).
[31] Y. Wang, B. Moritz, C.-C. Chen, T. P. Devereaux, and K. Wohlfeld, Phys. Rev. B **97**, 115120 (2018).
[32] H. Huang, C. Jia, Z. Chen, K. Wohlfeld, B. Moritz, T. Devereaux, W. Wu, J. Okamoto, W. Lee, M. Hashimoto, Y. He, Z. Shen, Y. Yoshida, H. Eisaki, C. Mou, C. Chen, and D. Huang, Scientific Reports **6**, 19657 (2016).
[33] J. Lamsal and W. Montfrooij, Phys. Rev. B **93**, 214513 (2016).
[34] S. J. Kawasaki, C. T. Lin, P. L. Kuhns, A. P. Reyes, and G.-Q. Zheng, Phys. Rev. Lett. **105**, 137002 (2010).
[35] Y. Y. Peng, J. Q. Meng, D. X. Mou, J. F. He, L. Zhao, Y. Wu, G. D. Liu, X. L. Dong, S. L. He, J. Zhang, X. Y. Wang, Q. J. Peng, Z. M. Wang, S. J. Zhang, F. Yang, C. T. Chen, Z. Y. Xu, T. K. Lee, and X. J. Zhou, Nat. Commun. **4**, 2459 (2013).
[36] J. Q. Meng, G. D. Liu, W. T. Zhang, L. Zhao, H. Y. Liu, W. Lu, X. L. Dong, and X. J. Zhou, Supercond. Sci. Technol. **22**, 045010 (2009).
[37] L. Zhao, W. T. Zhang, H. Y. Liu, J. Q. Meng, G. D. Liu, W. Lu, X. L. Dong, and X. J. Zhou, Chin. Phys. Lett. **27**, 087401 (2010).
[38] N. B. Brookes, F. Y. Harris, K. Kummer, A. Fondacaro, J. C. Cezar, D. Betto, E. Velez-Fort, A. Amorese, G. Ghiringhelli, L. Braicovich, R. Barrett, G. Berruyer, F. Cianciosi, L. Eybert, P. Marion, P. van der Linden, and L. Zhang, Nuclear Instruments and Methods in Physics Research Section A: Accelerators, Spectrometers, Detectors and Associated Equipment **903**, 175 (2018).
[39] L. Braicovich, M. M. Sala, L. J. P. Ament, V. Bisogni, M. Minola, G. Balestrino, D. D. Castro, G. M. D. Luca, M. Salluzzo, G. Ghiringhelli, and J. van den Brink, Phys. Rev. B **81**, 174533 (2010).
[40] N. S. Headings, S. M. Hayden, R. Coldea, and T. G. Perring, Phys. Rev. Lett. **105**, 247001 (2010).

[41] N. B. Christensen, H. M. Rønnow, D. F. McMorrow, A. Harrison, T. G. Perring, M. Enderle, R. Coldea, L. P. Regnault, and G. Aeppli, Proc. Natl. Acad. Sci. U.S.A. **104**, 15264 (2007).
[42] B. D. Piazza, M. Mourigal, N. B. Christensen, G. J. Nilsen, P. Tregenna-Piggott, T. G. Perring, M. Enderle, D. F. McMorrow, D. A. Ivanov, and H. M. Rønnow, Nat. Phys. **11**, 62 (2015).
[43] Y. Y. Peng, R. Fumagalli, Y. Ding, M. Minola, S. Caprara, D. Betto, G. M. D. Luca, K. Kummer, E. Lefrançois, M. Salluzzo, H. Suzuki, M. L. Tacon, X. J. Zhou, N. B. Brookes, B. Keimer, L. Braicovich, M. Grilli, and G. Ghiringhelli, Nat. Mater. **17**, 697 (2018).
[44] L. Braicovich, M. Minola, G. Dellea, M. L. Tacon, M. M. Sala, C. Morawe, J. C. Peffen, R. Supruangnet, F. Yakhou, G. Ghiringhelli, and N. B. Brookes, Rev. Sci. Instrum. **85**, 115104 (2014).
[45] M. Minola, Y. Lu, Y. Y. Peng, G. Dellea, H. Gretarsson, M. W. Haverkort, Y. Ding, X. Sun, X. J. Zhou, D. C. Peets, L. Chauviere, P. Dosanjh, D. Bonn, R. Liang, A. Damascelli, M. Dantz, X. Lu, T. Schmitt, L. Braicovich, G. Ghiringhelli, B. Keimer, and M. L. Tacon, Phys. Rev. Lett. **119**, 097001 (2017).
[46] R. Zeyher and A. Greco, Phys. Rev. B **87**, 224511 (2013).
[47] R. Blankenbecler, D. J. Scalapino, and R. L. Sugar, Phys. Rev. D **24**, 2278 (1981).
[48] S. R. White, D. J. Scalapino, R. L. Sugar, E. Y. Loh, J. E. Gubernatis, and R. T. Scalettar, Phys. Rev. B **40**, 506 (1989).
[49] Y. F. Kung, C.-C. Chen, Y. Wang, E. W. Huang, E. A. Nowadnick, B. Moritz, R. T. Scalettar, S. Johnston, and T. P. Devereaux, Phys. Rev. B **93**, 155166 (2016).
[50] E. W. Huang, C. B. Mendl, S. Liu, S. Johnston, H.-C. Jiang, B. Moritz, and T. P. Devereaux, Science **358**, 1161 (2017).
[51] M. Jarrell and J. E. Gubernatis, Phys. Rep. **269**, 133 (1996).
[52] K. Kurashima, T. Adachi, K. M. Suzuki, Y. Fukunaga, T. Kawamata, T. Noji, H. Miyasaka, I. Watanabe, M. Miyazaki, A. Koda, R. Kadono, and Y. Koike, Phys. Rev. B **121**, 057002 (2018).
[53] H.-C. Jiang and T. P. Devereaux, arXiv:1806.01465 (2018).